Electronic Supplementary Information for

One-Step Fabrication of Trimetallic Core-Shell Au@PdAuCu Mesoporous Nanospheres for Ethanol Electrooxidation

Hao Lv,[a] Lizhi Sun,[a] Xin Chen,[b] Dongdong Xu,[a,*] and Ben Liu[a,*]

[a]Jiangsu Key Laboratory of New Power Batteries, Jiangsu Collaborative Innovation Center of Biomedical Functional Materials, School of Chemistry and Materials Science, Nanjing Normal University, Nanjing 210023, China
[b]ME Genomic Inc., Software Industry Base, Shenzhen, 51806, China

*E-mails: ddxu@njnu.edu.cn (D. Xu); ben.liu@njnu.edu.cn (B. Liu)

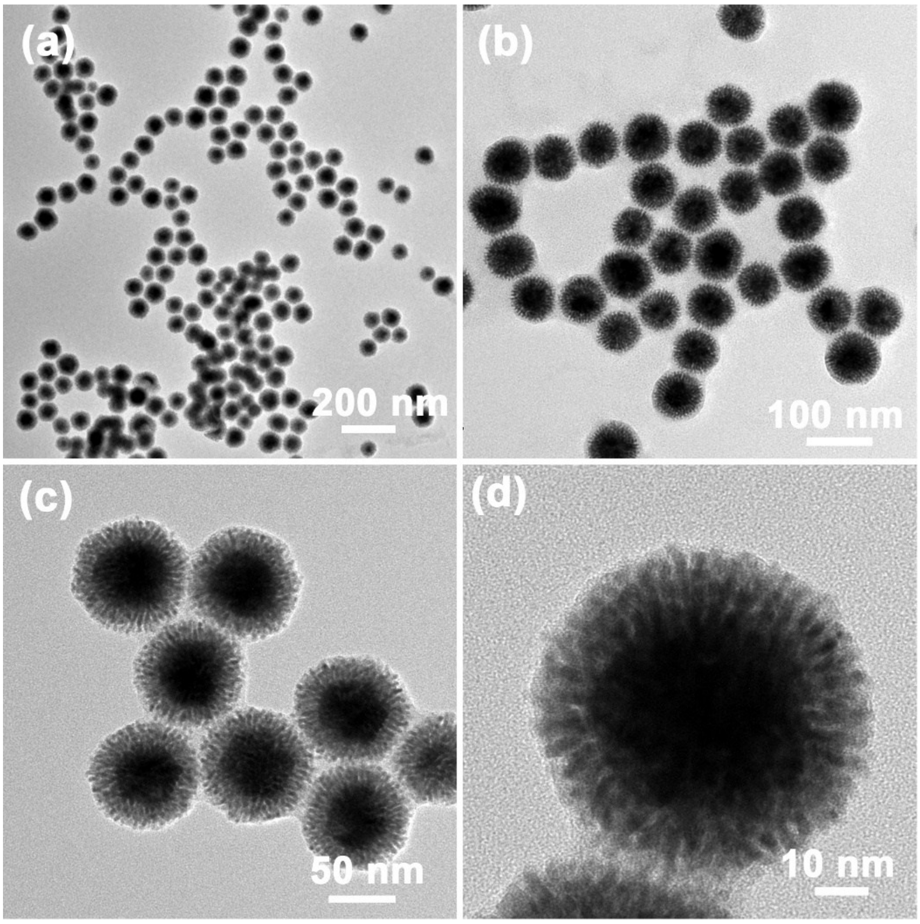

Fig. S1 Supporting TEM images of Au@PdAuCu-5 MNSs, indicating the monodispersed feature with an average diameter of ~85 nm.

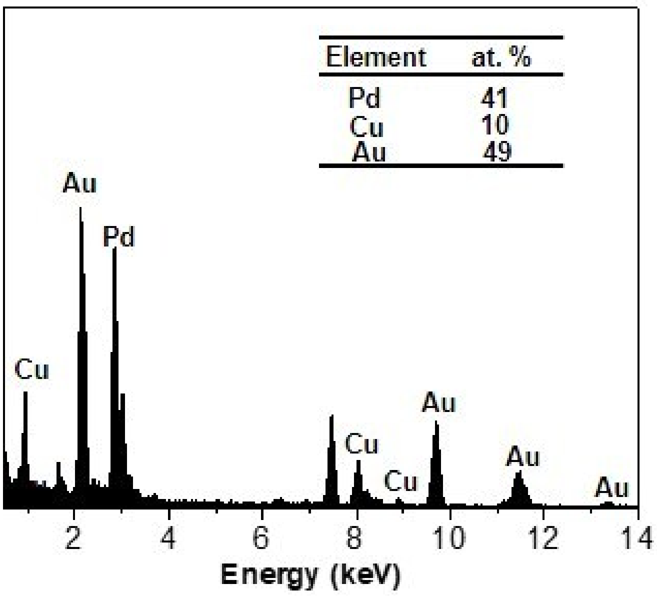

Fig. S2 EDS spectrum of core-shell Au@PdAuCu-5 MNSs.

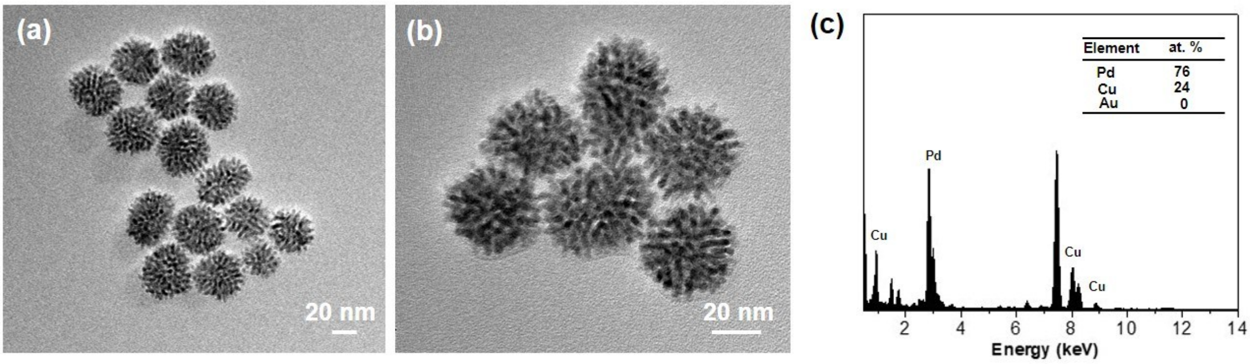

Fig. S3 (a, b) Supporting TEM images and (c) corresponding EDS spectrum of PdCu MNSs.

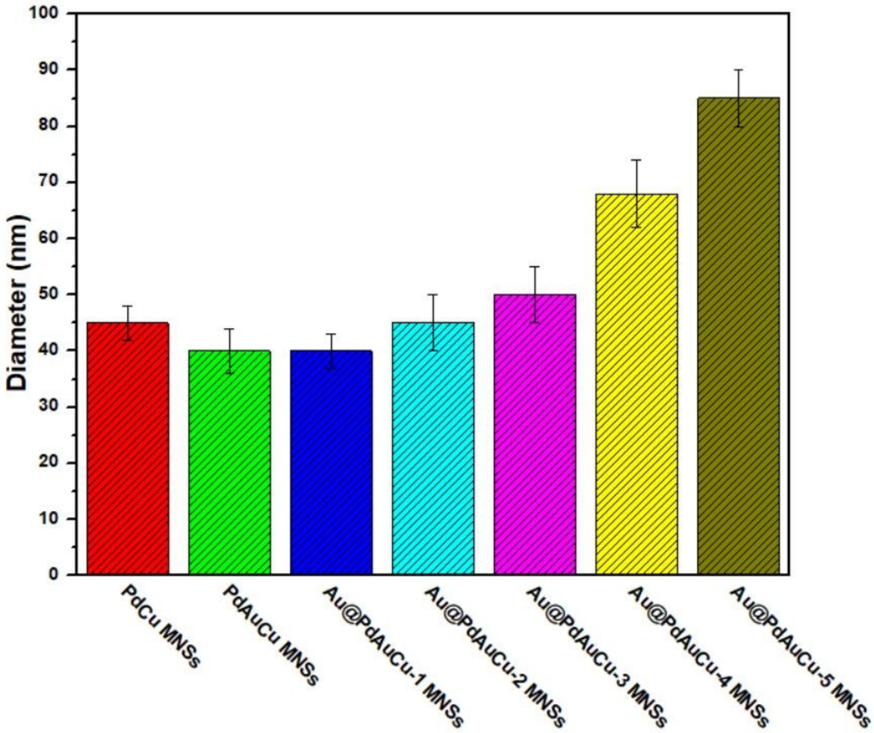

Fig. S4 The diameters of obtained metallic mesoporous nanospheres in this work.

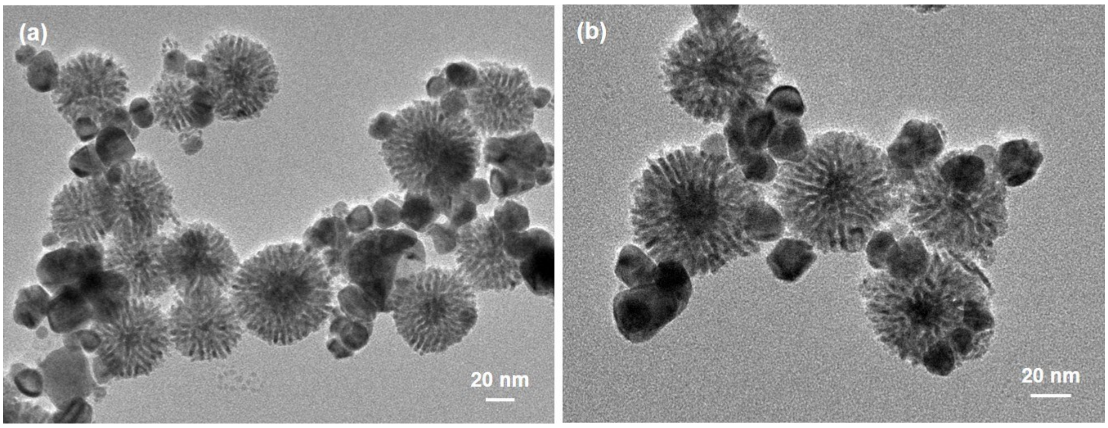

Fig. S5 TEM images of nanostructures obtained with the $HAuCl_4$ amount of more than 40 %.

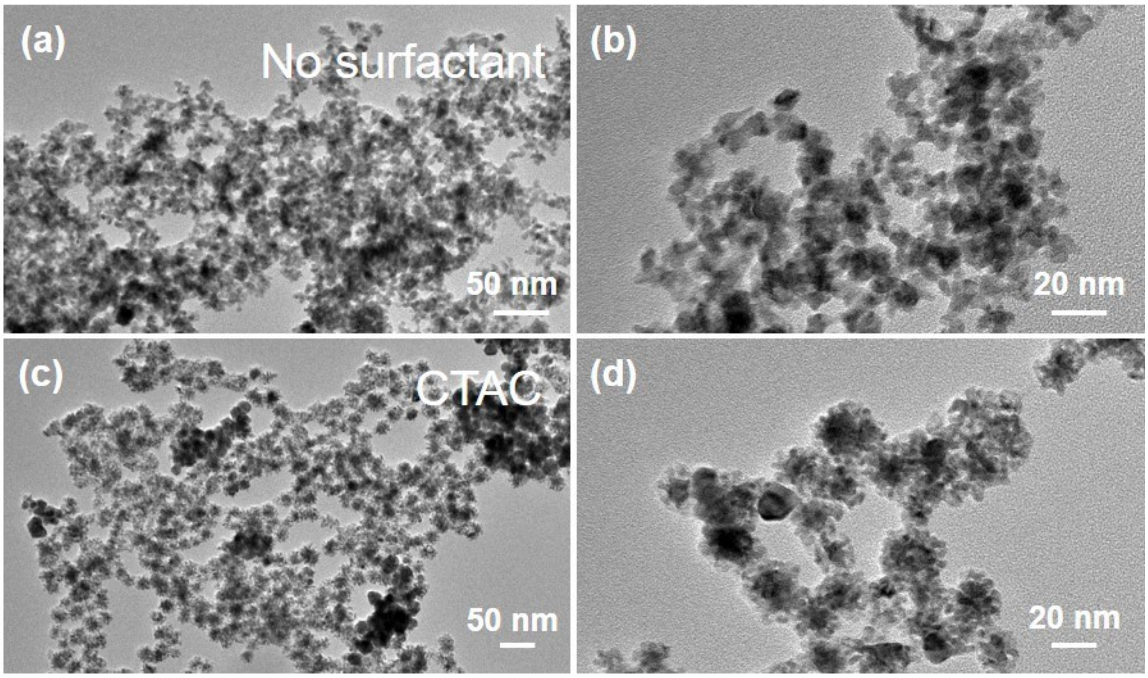

Fig. S6 TEM images of nanoparticles synthesized (a, b) without surfactant and (c, d) with surfactant of CTAC under the similar reactants to Au@PdAuCu MNSs-5 MNSs.

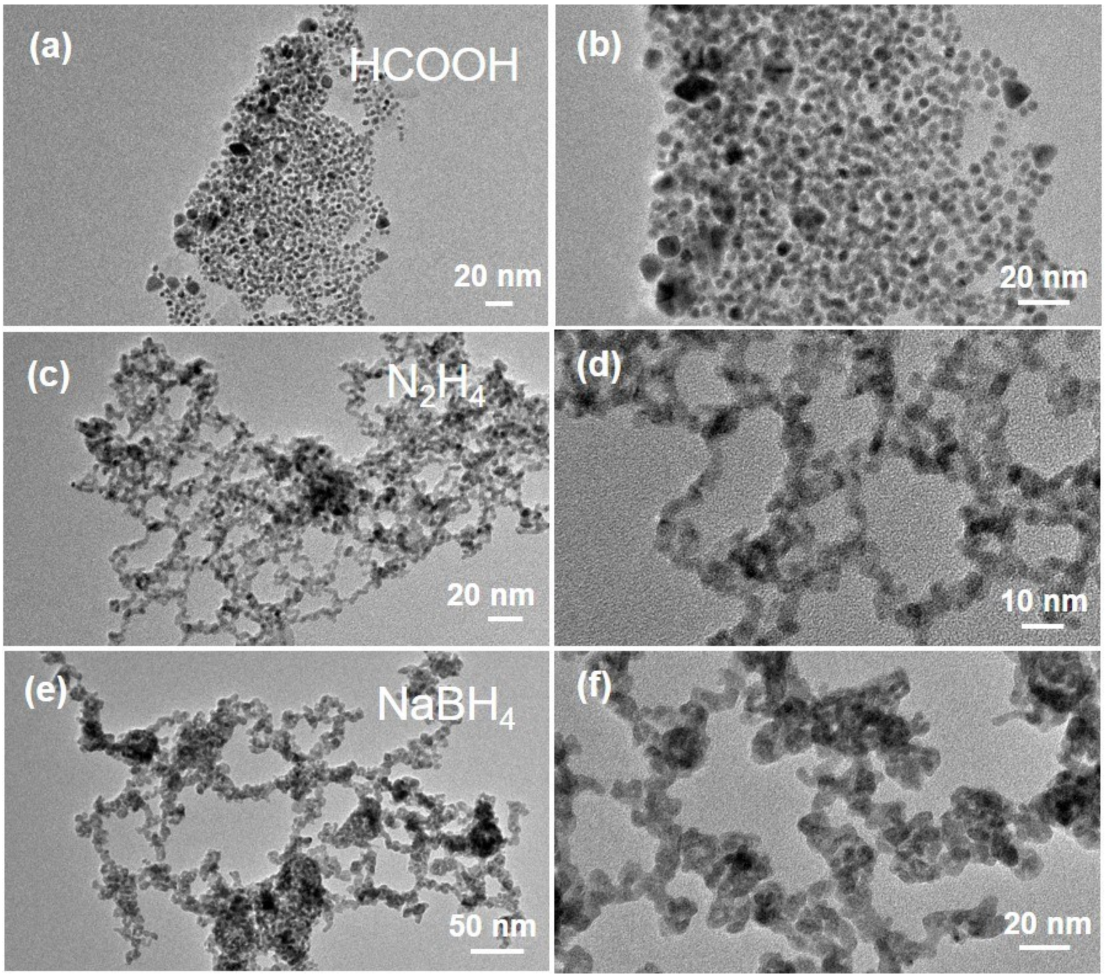

Fig. S7 TEM images of nanoparticles synthesized with the reducing agent of (a, b) formic acid (HCOOH), (c, d) hydrazine hydrate ($N_2H_4{\cdot}H_2O$), and (e, f) sodium borohydride ($NaBH_4$) under the similar reactants to Au@PdAuCu MNSs-5 MNSs.

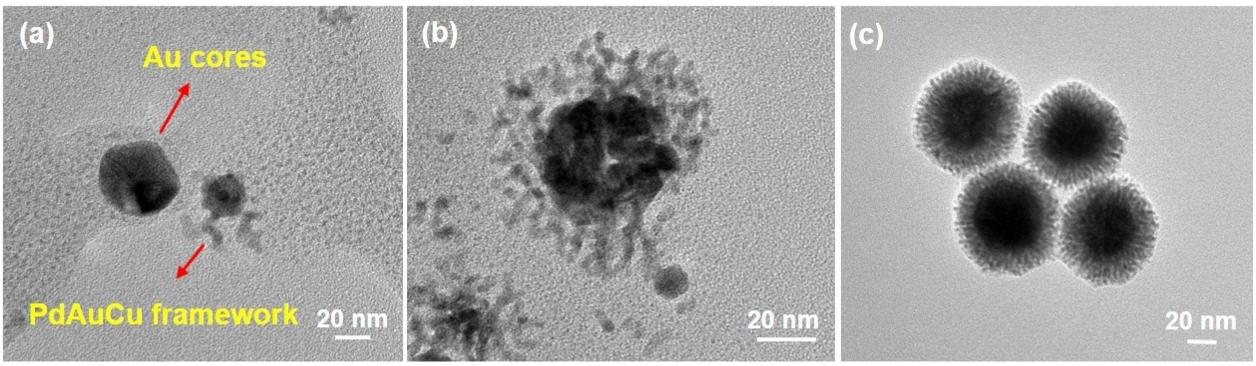

Fig. S8 (a, b) TEM images obtained in the initial stage of core-shell Au@PdAuCu-5 MNSs, and (c) TEM image of final Au@PdAuCu-5 MNSs. These observations demonstrated that Au cores firstly formed in the initial nucleation stage and PdAuCu frameworks gradually grew on the surfaces of Au nanocrystals.

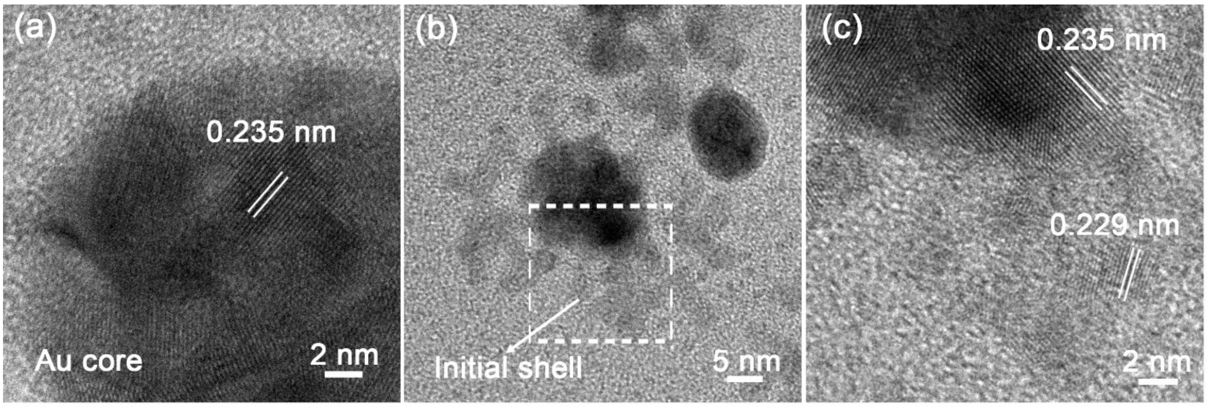

Fig. S9 (a) High-resolution TEM image of Au core, (b) high-magnification TEM image of initial shells, and (c) high-resolution TEM images of both Au core and PdAuCu shell. A lattice of 0.235 nm could be found in the initial nanoparticle, indicating the formation of elemental Au cores. The subsequent shell possess a lattice of ~0.229 nm, which could be indexed to trimetallic PdAuCu. These results further confirmed the formation of elemental Au cores and trimetallic PdAuCu shells.

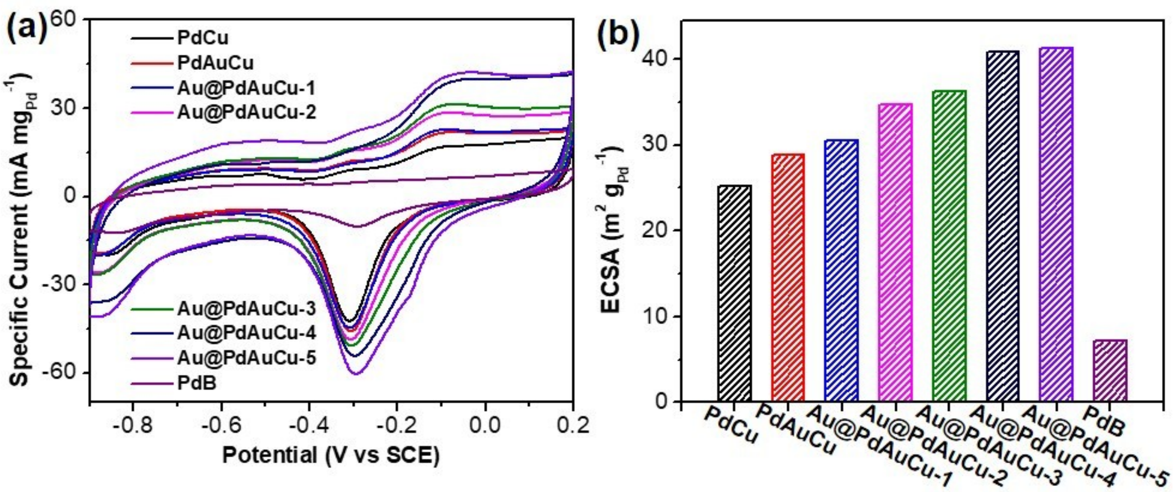

Fig. S10 (a) CV curves and (b) summarized ECSAs of PdCu MNSs, PdAuCu MNSs, Au@PdAuCu-1 MNSs, Au@PdAuCu-2MNSs, Au@PdAuCu-3 MNSs, Au@PdAuCu-4 MNSs, Au@PdAuCu-5 MNSs, and PdB collected in 1.0 M KOH with a scan rate of 50 mV s^{-1}.

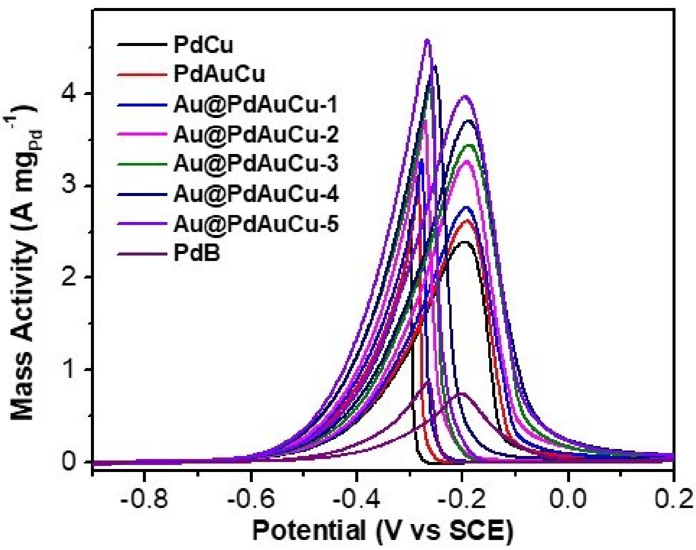

Fig. S11 CV curves of PdCu MNSs, PdAuCu MNSs, Au@PdAuCu-1 MNSs, Au@PdAuCu-2MNSs, Au@PdAuCu-3 MNSs, Au@PdAuCu-4 MNSs, Au@PdAuCu-5 MNSs, and PdB collected in 1.0 M KOH and 1.0 M ethanol with a scan rate of 50 mV s^{-1}.

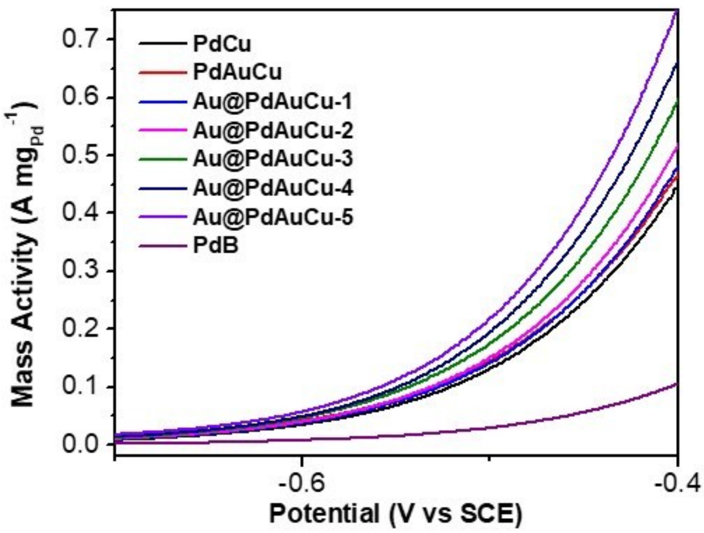

Fig. S12 Onset potentials of PdCu MNSs, PdAuCu MNSs, Au@PdAuCu-1 MNSs, Au@PdAuCu-2MNSs, Au@PdAuCu-3 MNSs, Au@PdAuCu-4 MNSs, Au@PdAuCu-5 MNSs, and PdB collected in 1.0 M KOH and 1.0 M ethanol.

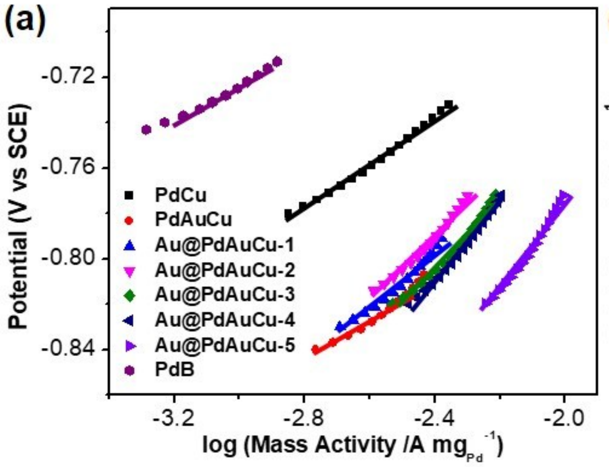

Fig. S13 Tafel plots of PdCu MNSs, PdAuCu MNSs, Au@PdAuCu-1 MNSs, Au@PdAuCu-2MNSs, Au@PdAuCu-3 MNSs, Au@PdAuCu-4 MNSs, Au@PdAuCu-5 MNSs, and PdB.

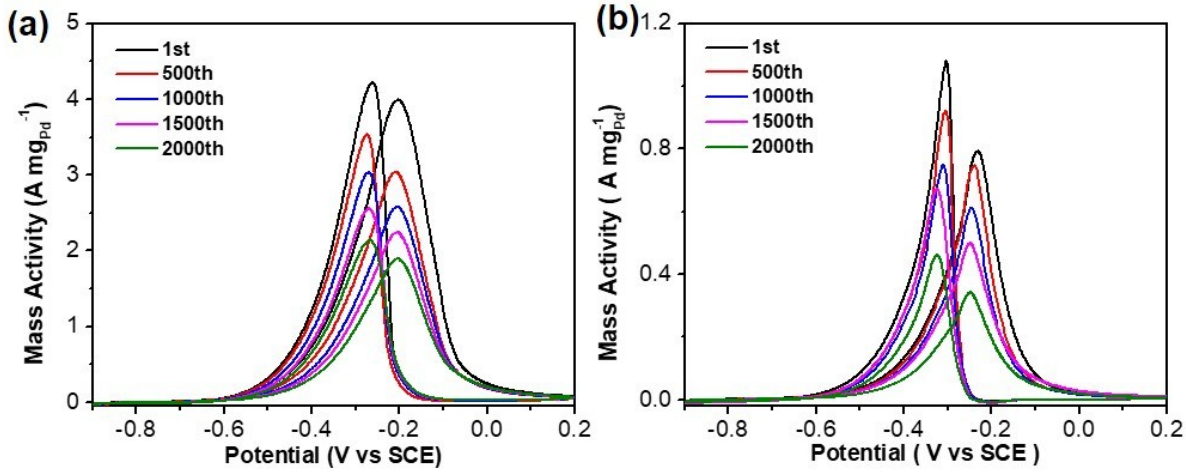

Fig. S14 CV curves of (a) Au@PdAuCu-5 MNSs and (b PdB) after 2000 successive scans.

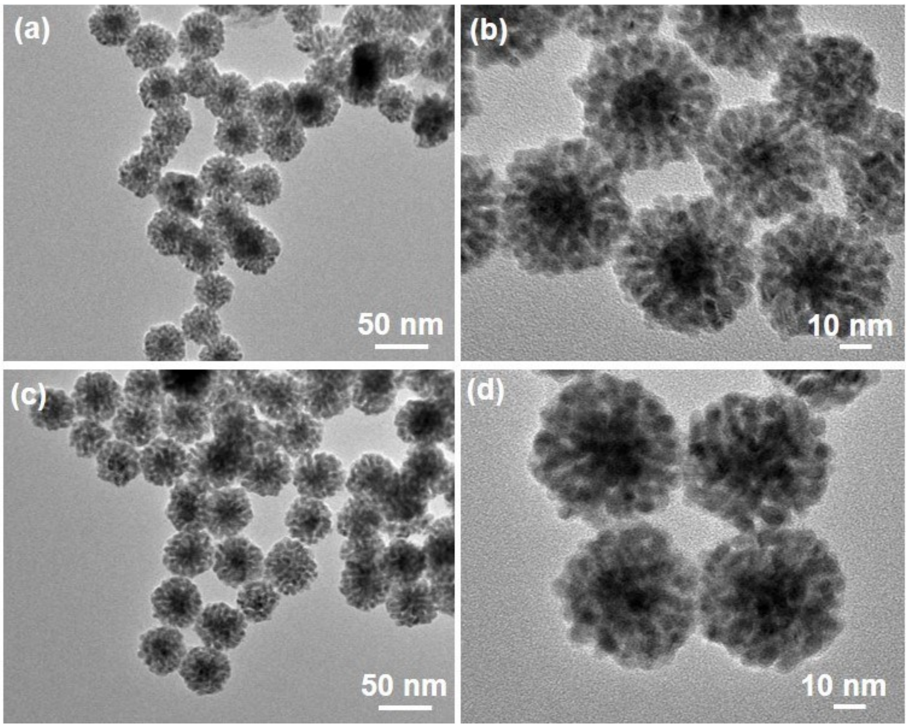

Fig. S15 TEM images of (a, b) core-shell Au@PdAu and (c, d) Au@PdAuAgCu MNSs.

Ethanol electrooxidation proceeds on Pd catalysts according to the following mechanisms:

$$Pd + CH_3CH_2OH + 3\ OH^- \rightarrow Pd - (CH_3CO)_{ads} + 3\ H_2O + 3\ e^- \quad (1)$$

$$Pd + OH^- \rightarrow Pd - OH_{ads} + e^- \quad (2)$$

$$Pd - (CH_3CO)_{ads} + Pd - OH_{ads} \rightarrow Pd - CH_3COOH + Pd \quad (3)$$

$$Pd - CH_3COOH + OH^- \rightarrow Pd + CH_3COO^- + H_2O \quad (4)$$

The rate-determining step of electrochemical EOR is the oxidation/removal of poisoning carbonaceous intermediates on Pd (Pd-$(CH_3CO)_{ads}$) by adsorbed OH (OH_{ads}) (Eq. 3). For core-shell Au@PdAuCu MNSs, strictly speaking, all of three metals (Pd, Au, Cu) act as the active sites simultaneously, although they possess different roles for ethanol electrooxidation. First, ethanol was oxidized on Pd atoms into carbonaceous intermediates of $(CH_3CO)_{ads}$ which strongly adsorbed on Pd (Pd-$(CH_3CO)_{ads}$) to inactivate the Pd catalyst. By contrast, oxophilic metals of Au and Cu can effectively facilitate the adsorption and formation of OH_{ads} by Au-OH_{ads} and Cu-OH_{ads}. Therefore, the reaction between Pd-$(CH_3CO)_{ads}$ and Au-OH_{ads}/Cu-OH_{ads} kinetically accelerates the reaction/removal of $(CH_3CO)_{ads}$ and thus improves electrocatalytic performance (bifunctional effect). Besides, alloying Pd with Au and Cu could greatly change the electron energy state and reduce the adsorption energy of $(CH_3CO)_{ads}$ on Pd atoms (electronic effect).

Table S1. Summarization of electrochemical EOR performance of different electrocatalysts in alkaline solution.

Electrocatalyst	Electrolyte		Peak current from CV ($mA\ mg^{-1}$)	Reference
	Ethanol	KOH	50 mV s^{-1}	
Au@PdAuCu MNSs	1 M	1M	3990	This work
PdCo nanotube /carbon cloth	1 M	1 M	~1500	Angew. Chem. Int. Ed. 2015 , 54 , 3669
Au@AgPd Nanoparticles	1 M	1 M	1160	J. Phys. Chem. C 2015, 119, 18434
Au@Pd Core–Shell Nanorods	1 M	1 M	2920	Adv. Mater. 2017, 29, 1701331
PdAg hollow nanoflowers	1 M	1 M	1616	Chem. Eur. J. 2016, 22, 16642
$PdCu_2$ Nanoparticles	1 M	1 M	1600	ACS Appl. Mater. Interfaces 2016, 8, 34497
PdCu nanocapsules	1 M	1 M	1140	Nanoscale, 2014, 6, 2768
Pd_4Au_1 -P/CNT	1 M	1 M	2296	J. Catal. 2017, 353, 256
Pd_1Ag_1 NPs/GO	1 M	1 M	1601	J. Power Sources 2014, 263, 13.
PdCo/N-doped Cabon	1 M	1 M	1250	J. Mater. Chem. A 2017, 5, 10876
PdNi Hollow Nanospheres	1 M	1 M	3630	Angew. Chem. Int. Ed. 2015, 54, 1310
Pd/Ru nanodendrites	1 M	1 M	1150	Nanoscale 2015, 7, 12445
Pd-$NiCoO_x$ /C	1 M	0.5 M	~450	J. Power Sources 2015, 273, 631
10.8-nm-thick PdPt NWs	0.5 M	1 M	940	Adv. Mater. 2012, 24, 2326
Pd_7/Ru_1 nanodendrites	1 M	1 M	~1150	Nanoscale 2015, 7, 12445